Supplement of The Cryosphere, 20, 67–86, 2026
https://doi.org/10.5194/tc-20-67-2026-supplement

The Cryosphere Open Access EGU

Supplement of

Quantifying degradation of the Imja Lake moraine dam with fused InSAR and SAR feature tracking time series

George Brencher et al.

Correspondence to: George Brencher (gbrench@uw.edu)

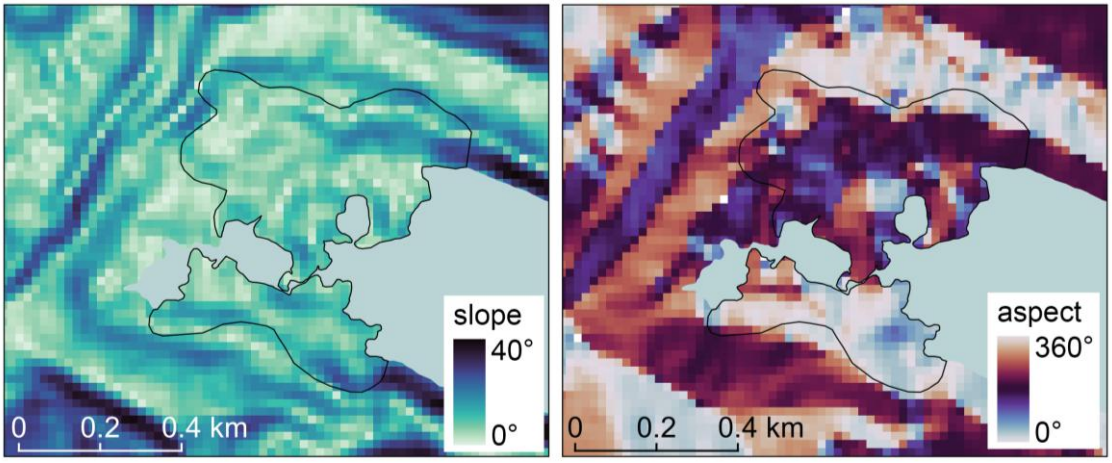

Figure S1: Surface slope (left) and aspect (right) of the Imja Lake moraine dam from the COP30 composite digital elevation model prepared from TSX/TDX scenes acquired between 2011 and 2015 (European Space Agency, 2022).

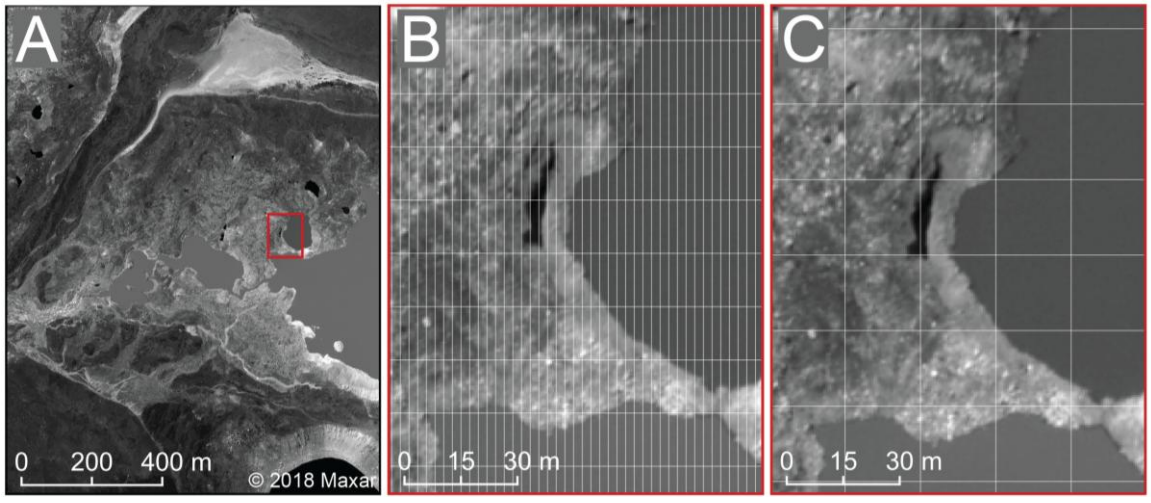

Figure S2: Illustration of Sentinel-1 product resolution over the Imja Lake moraine dam. (A) Maxar WorldView-1 panchromatic orthoimage from June 19, 2018 (Catalog ID 10200100758B9800) with 0.53 m ground sample distance. (B) Detail of pond and lake margin denoted by red box in A, with 14.1 by 2.3 m grid overlaid showing native Sentinel-1 single-look complex (SLC) azimuth and range resolution, respectively. (C) Same as B, with 20 by 20 m grid showing the pixel spacing of our combined interferometric synthetic aperture radar (InSAR) and feature tracking products.

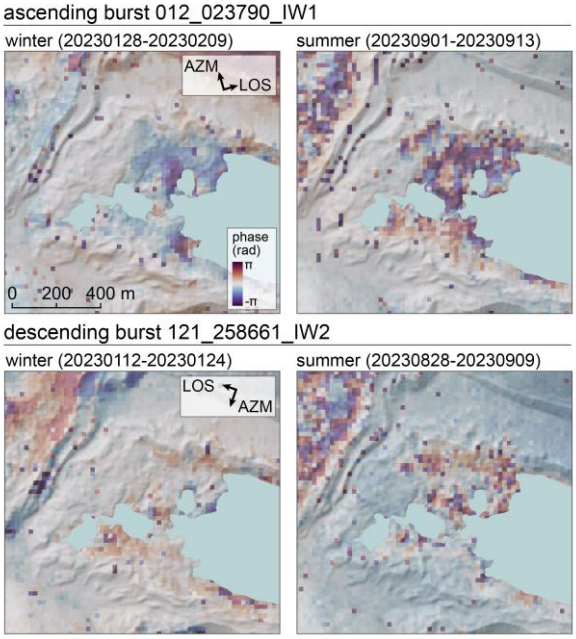

Figure S3: Examples of wrapped interferograms. Note that no local reference point has been set for these interferograms, and they still contain some atmospheric noise over the moraine dam.

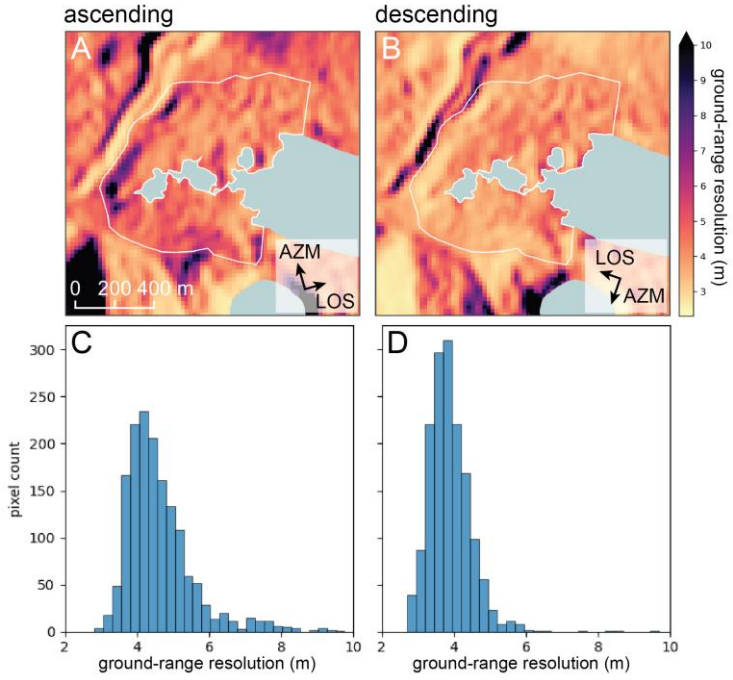

Figure S4: Ground-range resolution of ascending (A) and descending (B) SLCs. C and D show the distribution of ground-range resolution values for pixels over the moraine dam (white outline).

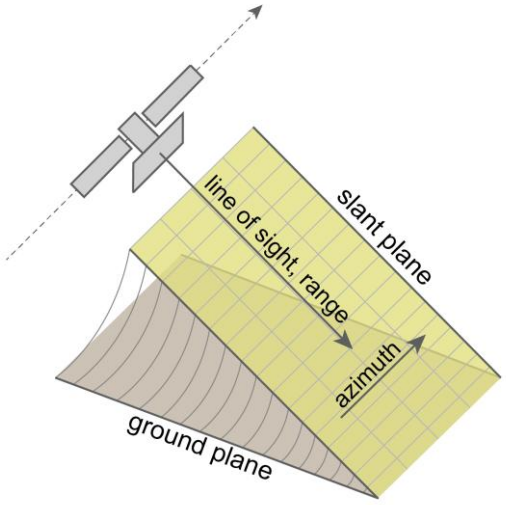

Figure S5: SAR acquisition geometry.

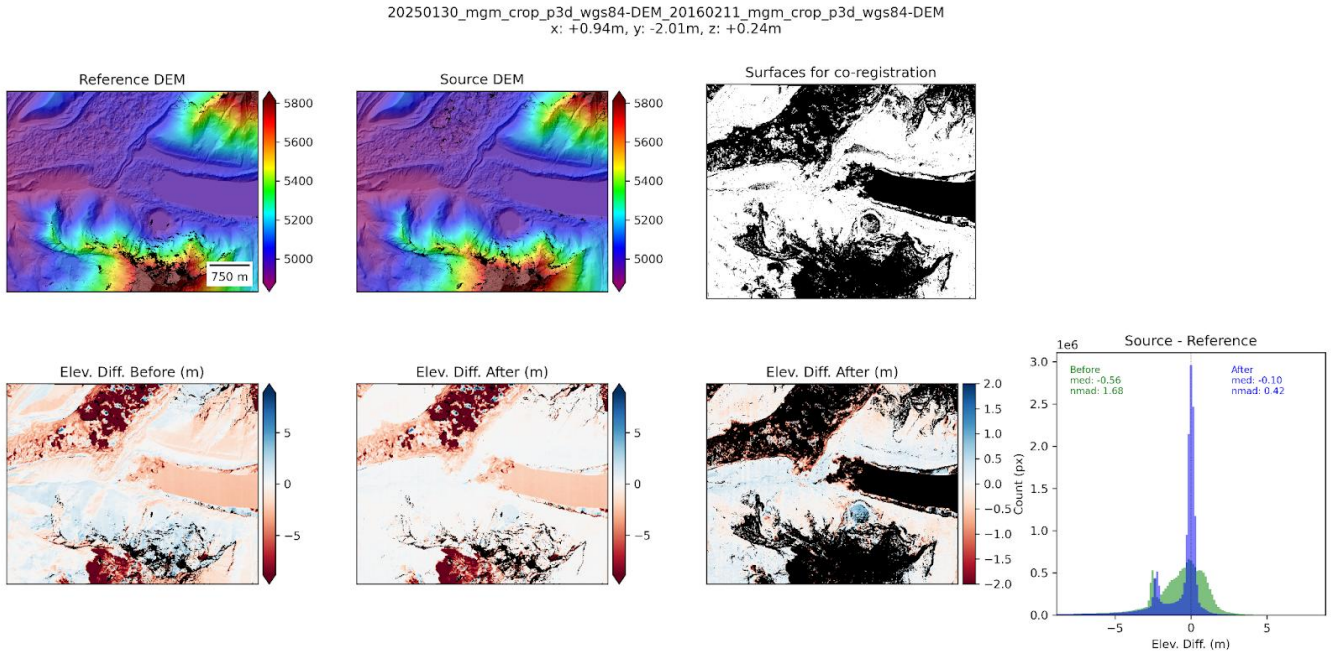

Figure S6: Co-registration results for the February 11, 2016 DEM (reference) and January 30, 2025 DEM (source). The latter was shifted (+0.94 m, -2.01 m, +0.24 m, see title) to minimize residuals over unmasked surfaces (white in the top right figure). Bottom row shows elevation difference maps before co-registration (left), and after co-registration (center). Bottom right map shows enhanced color stretch and histogram shows unmasked values before and after co-registration. Note that some large negative values (-5 to -2.5 m) observed for unmasked pixels near glacier margins are included in the histogram, but these outliers did not affect the robust co-registration.

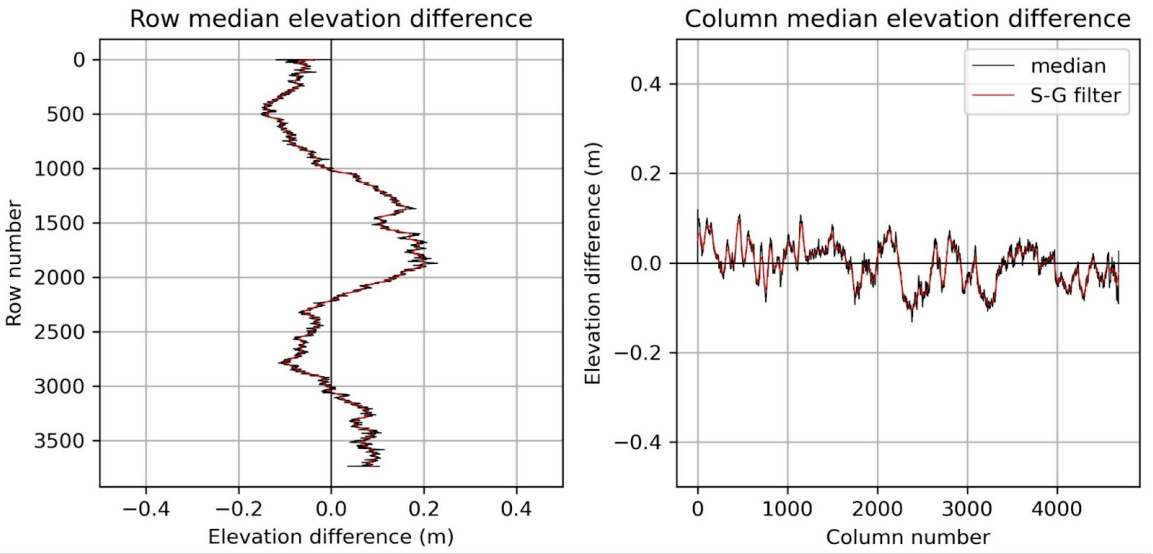

Figure S7: Row (left panel) and column (right panel) median elevation difference values (black) over static control surfaces after DEM co-registration (see Figure S6), showing residual artifacts due unmodeled attitude error ("jitter", left) and detector array geometry calibration (right). See Shean et al. (2016) and the "ct_at_correction_wrapper" function of demcoreg/coreglib.py for more details. Red line shows the smoothed model from a Savitzky-Golay filter, which was used to correct all rows and columns in the unmasked elevation difference product.

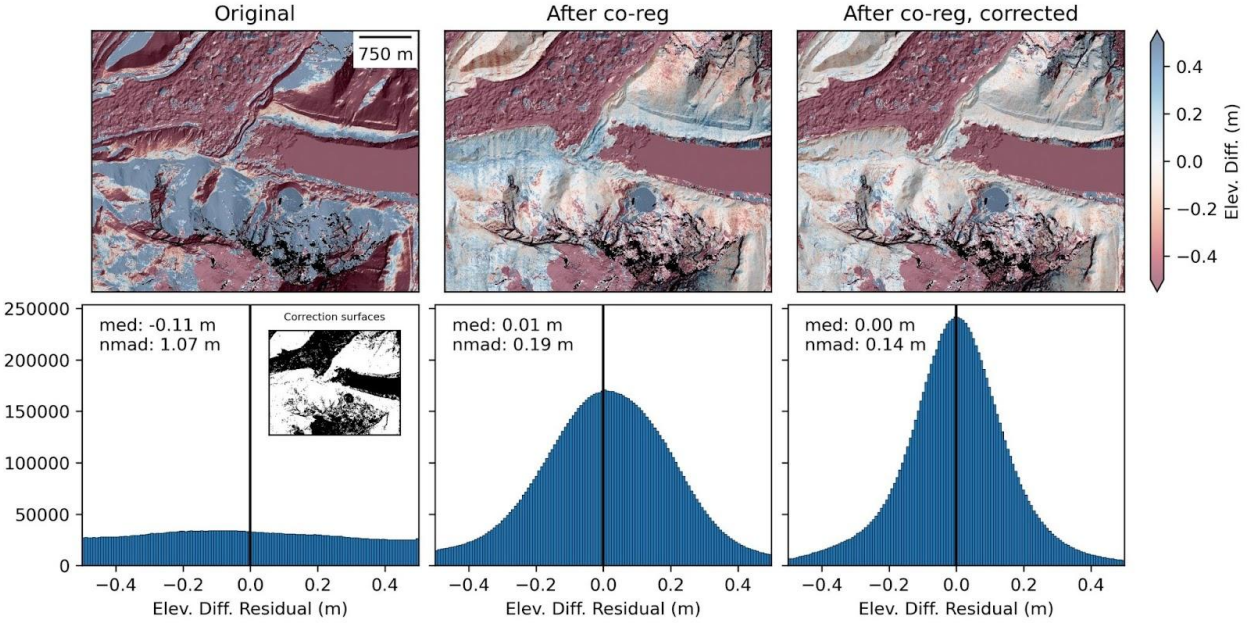

Figure S8: Elevation difference maps (top row) and histograms (bottom row) of residuals over exposed surfaces (white areas in inset axes of bottom left panel) assumed to have no elevation change during the study period. Left shows original difference map, center shows difference map after co-registration, right shows final difference map after co-registration and correction of row/column median values.

Section S1: Expected ice flow

We computed the expected surface-parallel velocity (u_s) due to internal deformation of buried ice using a simple 1-D model with no basal sliding (Eq. 8.35 in Cuffey & Paterson, 2010):

$$u_s = \frac{2A}{n+1}\tau_b{}^n H \quad \text{(S1)}$$

where A is a flow rate factor (typically $2.4*10^{-24}$ $s^{-1}Pa^{-3}$ for temperate glacier ice), n is the flow law exponent (3), H is the ice thickness, and τ_b is the basal shear stress, defined as:

$$\tau_b = \rho g H \sin(\theta) \quad \text{(S2)}$$

where ρ is ice density (917 kg m^{-3}), g is acceleration due to gravity (9.81 m s^{-2}), H is ice thickness, and θ is surface slope. We computed expected surface-parallel velocity due to ice flow for a range of ice thicknesses (0-70 m) and surface slope values (0-20°) for the Imja Lake moraine dam.

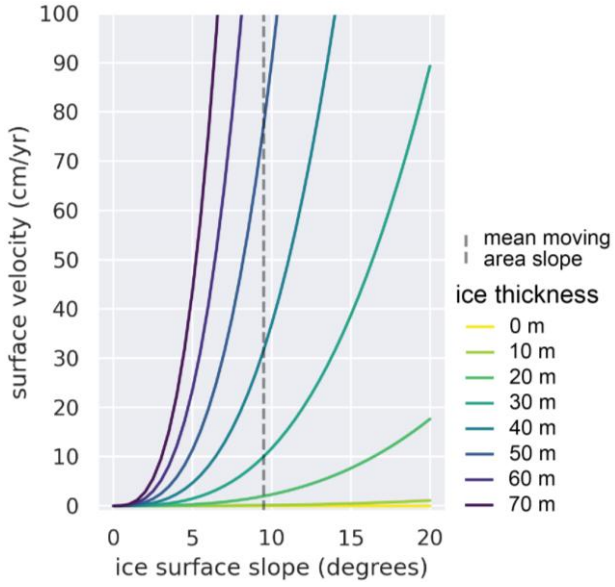

Figure S9: Expected along-slope surface velocity due to internal deformation (no sliding) of temperate glacier ice (Eq 8.35 in Cuffey & Paterson, 2010) for a range of ice thicknesses and surface slope for the Imja Lake moraine dam.

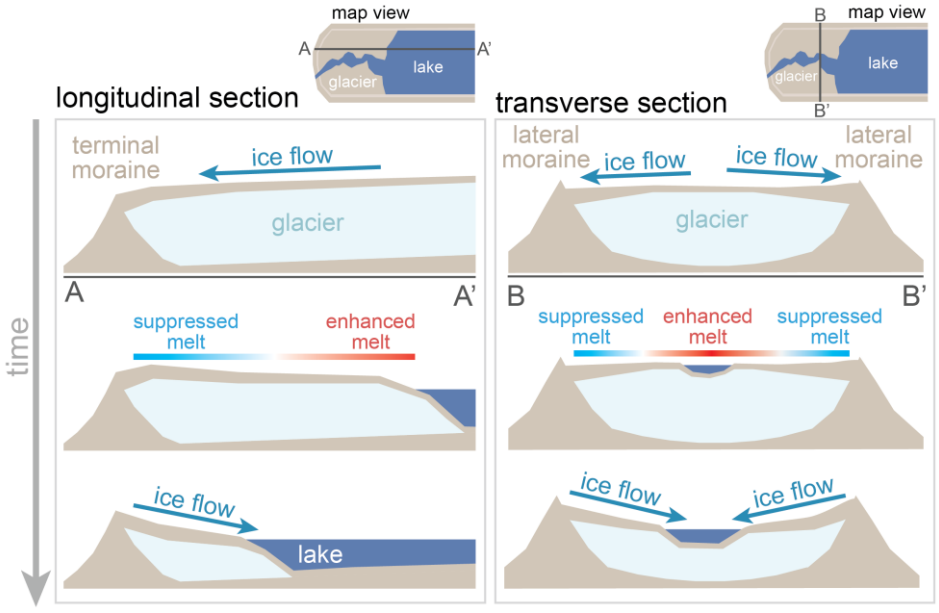

Figure S10: Schematic showing topographic inversion at the Imja Lake moraine dam. Melt is enhanced at the lake edges through interaction with liquid water and ice cliff retreat. Melt is suppressed near the lateral moraines due to insulation from thicker debris and the effects of local shading.

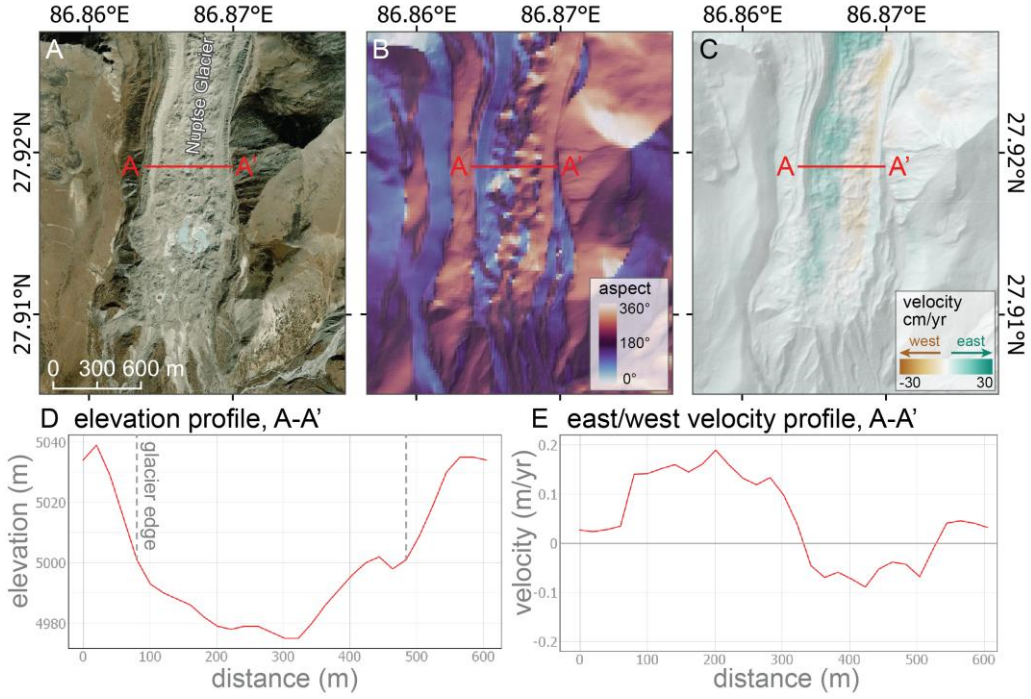

Figure S11: The Lower Nuptse Glacier, located to the west-northwest of Imja Lake. Note the general surface aspect (B), concave-up transverse profile (D) and pattern of surface motion toward the glacier centerline (C/E).

Section S2: LOS decomposition bias

To investigate potential bias caused by the assumptions made for our LOS decomposition (Section 4.3), we used the observed north/south velocity measurements from the DEM-derived validation data (Section 4.4, Fig. 3) to estimate the expected bias in the east/west and vertical velocity components from our decomposition. To do this, we solved the following equations for vertical and east/west velocity:

$$v_{asc} = v_{ud}\hat{\boldsymbol{l}}_{asc} \cdot \hat{\boldsymbol{l}}_{ud} + v_{ew}\hat{\boldsymbol{l}}_{asc} \cdot \hat{\boldsymbol{l}}_{ew} + v_{ns}\hat{\boldsymbol{l}}_{asc} \cdot \hat{\boldsymbol{l}}_{ns} \quad \text{(S3)}$$

$$v_{des} = v_{ud}\hat{\boldsymbol{l}}_{des} \cdot \hat{\boldsymbol{l}}_{ud} + v_{ew}\hat{\boldsymbol{l}}_{des} \cdot \hat{\boldsymbol{l}}_{ew} + v_{ns}\hat{\boldsymbol{l}}_{asc} \cdot \hat{\boldsymbol{l}}_{ns} \quad \text{(S4)}$$

Where $\hat{\boldsymbol{l}}$ represents a unit vector, v is the mean velocity over the study period, and the subscripts (*asc*, *des*, *ud*, *ew*, and *ns*) correspond to the ascending, descending, up/down, east/west, and north/south components, respectively. The v_{asc} and v_{des} values are the mean ascending and descending LOS velocity magnitude from our combined InSAR and feature tracking time series approach. For this analysis we substitute the north/south velocity from the DEM-derived validation data as the v_{ns} value in each equation. Thus, rather than assuming that the v_{ns} north/south contribution to the LOS velocity is 0, as in Section 4.3, here we include the observed north/south velocity magnitude when solving for the v_{ud} and v_{ew} components (Fig. S12).

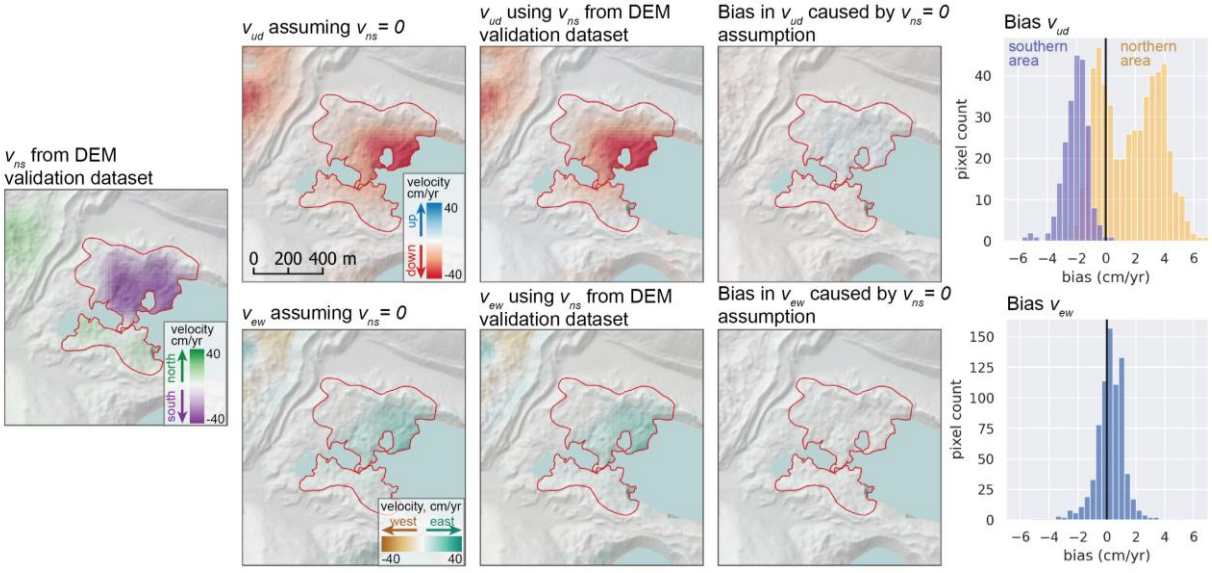

Figure S12: Estimated bias in up/down and east/west velocity components caused by ignoring the north/south velocity in the LOS decomposition. *v* is the mean velocity over the study period, and the subscripts (*ud*, *ew*, and *ns*) correspond to the up/down, east/west, and north/south components, respectively. (left) The north/south velocity components from the DEM-derived validation dataset. (Second column) The up/down and east/west velocity components, assuming that the north/south velocity component is 0. (Center column) The up/down and east/west velocity components calculated using the north/south velocity component from the DEM-derived validation dataset. (Fourth column and right column) Difference maps and histograms showing estimated bias caused by neglecting the north/south velocity component. Expected bias over the moving area is small (~ 3-4%) compared to signal magnitude.

The DEM-derived validation data show that the northern portion of the moraine dam was moving southward, with a mean velocity of -19 cm yr^{-1}, while the southern portion of the moraine dam was moving northward, with a mean velocity of 7 cm yr^{-1}. Including these displacements during the LOS decomposition leads to a slight underestimation of the vertical velocity magnitude over the northern portion (mean bias of 1.6 cm yr^{-1} or ~ 10%) and a slight overestimation of the vertical velocity magnitude over the southern portion (mean bias of -2.1 cm yr^{-1} or ~ 35%). When averaged over the entire moving area, these biases largely cancel, with a mean total bias of +0.6 cm yr^{-1}, or ~ 4% of the observed mean vertical velocity from the DEM-derived validation data. In the east/west direction, including the true north/south displacements results in a slight overestimation of eastward velocity (mean bias of 0.2 cm or 3% of the observed mean east/west velocity from the DEM-derived validation data.

We next address the question of whether the "downward signal" observed during the warm season could be caused by north/south displacement. To do this, we calculated the change in north/south velocity that would be required to produce the observed magnitude of seasonal change in vertical velocity (-8.0 cm yr^{-1}). We first subtracted the January/February vertical velocity (Fig. 8) from our September/October vertical velocity to quantify the observed seasonal change in vertical velocity. We then projected this observed vertical seasonal change into the ascending LOS, and calculated the theoretical magnitude of north/south velocity change that would be required to achieve the same change in ascending LOS velocity.

The seasonal change in velocity over the moving area can either be explained by a -8.0 cm/yr change in the mean vertical velocity or a +62 cm yr^{-1} change in the mean north/south velocity (Fig. S13). A much larger change in the north/south velocity is needed because Sentinel-1 LOS measurements are largely insensitive to north/south motion. Within the moving area, some pixels would require a northward change in velocity of more than 3 m yr^{-1}. The -8.0 cm yr^{-1} mean vertical change is much more realistic, and can be explained by the well-documented physical process of seasonal ice melt in these areas (Irvine-Fynn et al., 2011). The alternative explanation would require a large seasonal transition to *rapid*, *upslope* motion over most of the moraine dam moving area, which has no physical basis and is inconsistent with the DEM-derived validation data.

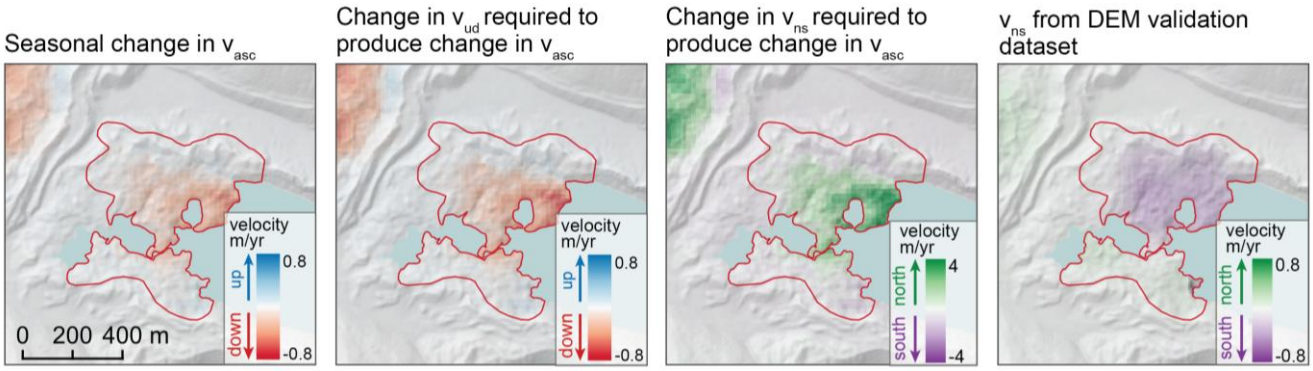

Figure S13: Observed seasonal change in ascending LOS velocity (left) and the corresponding change in vertical (second left) or north/south velocity (second right) required to produce the same LOS seasonal change. *v* is velocity, and the subscripts (*asc*, *ud*, and *ns*) correspond to the ascending LOS, up/down, and north/south directions, respectively. Note the expanded color bar range for the north/south velocity plot. The required change in the vertical direction has a much smaller magnitude than the required change in velocity in the north/south direction, as the LOS vector has a small northward component. The required change in velocity in the north/south direction is inconsistent with the observed north/south velocity from the DEM-derived validation data (right).

References

Cuffey, K. M., and Paterson, W. S. B.: The Physics of Glaciers (Fourth Edition), Butterworth-Heinemann, 2010.

Irvine-Fynn, T. D. L., Barrand, N. E., Porter, P. R., Hodson, A. J., and Murray, T.: Recent High-Arctic glacial sediment redistribution: A process perspective using airborne lidar, Geomorphology, 125(1), 27–39, https://doi.org/10.1016/j.geomorph.2010.08.012, 2011.

Shean, D. E., Alexandrov, O., Moratto, Z. M., Smith, B. E., Joughin, I. R., Porter, C., and Morin, P.: An automated, open-source pipeline for mass production of digital elevation models (DEMs) from very-high-resolution commercial stereo satellite imagery, ISPRS J. Photogramm. Remote Sens., 116, 101–117, https://doi.org/10.1016/j.isprsjprs.2016.03.012, 2016.